RSC Applied Polymers

ROYAL SOCIETY OF CHEMISTRY

PAPER

View Article Online
View Journal

Cite this: DOI: 10.1039/d5lp00361j

Imidazolium-mediated poly(ionic liquid) hydrogels for multifunctional pollutant removal systems

Muhammed Yoosuf,[a] Zhaksylyk Suiindik,[a] Sudhir Ravula,[b] Jason E. Bara [b] and Irshad Kammakakam *[a]

Hydrogels, cross-linked polymer networks that swell enormously in water, have remarkably garnered significant attention as promising materials for various applications such as biomedical engineering, soft robotics, and environmental separation processes. In this study, we report the design and synthesis of imidazolium-mediated poly(IL) hydrogels as multifunctional materials for a wide-range of applications, including high pollutant removal efficiency, enhanced dye adsorption, and controlled drug delivery. To achieve our goal, we have strategically developed a photo-polymerizable bisimidazole monomer featuring three units of ethylene glycol (EG) chain as a spacer between two imidazole rings with a terminal vinyl group. The rational design of crosslinked network architectures within the imidazolium poly(IL) matrix has been exclusively targeted, whereby choosing an appropriate cross-linker, such as poly(ethylene glycol) diacrylate (PEGDA), is anticipated to enhance the performance of the resultant hydrogels. Imidazolium crosslinking at three weight percentage levels affected the physical properties and performance of newly developed hydrogel matrices, which were extensively characterized by Fourier-transform infrared (FT-IR) spectroscopy, thermogravimetric analysis (TGA), and scanning electron microscopy (SEM), as well as their swelling and adsorption properties. Interestingly, the newly developed imidazolium-mediated poly(IL)-derived hydrogels exhibited outstanding adsorption and removal efficiency for both anionic dyes and pharmaceutical products from the aqueous medium. Precisely, while mercuric ($HgCl_2$) adsorption exhibited complete separation with a q_{max} value of 217.5 mg g^{-1}, methyl orange (MO) showed adsorption with a q_{max} value of 158.73 mg g^{-1}, revealing the remarkable ability of the newly developed imidazolium-mediated poly(IL) hydrogels to remove pollutants from water. Furthermore, the hydrogel with the optimal composition, [$BImEG_3$/PEGDA] [30 : 70], exhibited a good adsorption capacity of 127.22 mg g^{-1} for sodium diclofenac (DCl), presenting an interesting platform for both dye and drug adsorption systems.

Received 17th November 2025,
Accepted 13th March 2026

DOI: 10.1039/d5lp00361j

rsc.li/rscapplpolym

1. Introduction

Hydrogels are three-dimensional networks of hydrophilic substances, such as polymers,[1–4] peptides,[5–7] polysaccharides,[8–10] and other molecular building blocks,[11–14] that can absorb and retain large amounts of water or biological fluids without changing shape.[15] These materials have proven to be very useful in various biomedical, environmental, and industrial applications because their physicochemical properties can be controlled, allowing them to mimic the natural tissue environment.[16] Network structures in hydrogels are formed through either covalent or non-covalent crosslinking of small molecules or polymeric substances, which enable them to swell and retain substantial volumes of water or biological fluids while maintaining their overall integrity and preventing disintegration.[17] The design of these materials involves selecting synthetic or natural polymers, employing various crosslinking techniques, and incorporating stimuli-sensitive features that enable hydrogels to respond to environmental stimuli, such as temperature, pH, or biochemical signals.[18] Recent advances have led to the creation of composite and nanocomposite hydrogels, where nanoparticles or functional additives are integrated, significantly enhancing their mechanical strength, biocompatibility, and multifunctionality. This expansion allows their use in catalysis, electronics, biosensing, and, most notably, in biomedicine as drug delivery systems and tissue engineering scaffolds.[19] These well-designed hydrogels can mimic the extracellular matrix, promote cell proliferation, and deliver therapy in a controlled manner, positioning them as key players in regenerative medicine, as well as in environmental and agricultural applications such as water management and nutrient preservation.[20] As the field progresses, new structures such as triple-network and self-healing hydrogels

[a]Department of Chemistry, Nazarbayev University, 53 Kabanbay Batyr Ave, 01000 Astana, Kazakhstan. E-mail: irshad.kammakakam@nu.edu.kz
[b]University of Alabama, Department of Chemical & Biological Engineering, Tuscaloosa, AL 35487-0203, USA

are emerging, offering greater toughness and resilience and expanding the potential of these materials in both clinical and industrial settings.

Polymeric hydrogels exhibit a wide range of design strategies, all of which aim to optimize their structure and function for more advanced applications. One such key design involves stimuli-responsive hydrogels, which alter their properties in response to external stimuli such as pH, temperature, or ionic strength, thereby rendering them more applicable in tissue engineering and controlled drug release systems.[21] Another important design involves the fabrication of double-network (DN) hydrogels, where two interpenetrating polymer networks are incorporated to significantly improve mechanical strength and toughness, often utilizing natural polysaccharides or synthetic polymers for enhanced biocompatibility and tunable functionality.[22] Hollow-structured hydrogels, inspired by nature's hollow systems, are fabricated based on supramolecular interactions and applied as advanced soft actuators or reactors for chemical reactions due to their complex three-dimensional structures.[23] Further design complexity is introduced by self-healing hydrogels, which utilize dynamic covalent or coordination bonds, specifically metal–ligand interactions, for reversible network formation, thereby enabling them to be injectable and suitable for minimally invasive procedures.[24] Nanocomposite hydrogels, which feature the inclusion of nanoparticles comprising carbon-based, metallic, or polymeric materials in hydrogel matrices, offer enhanced mechanical, electrical, and responsive properties for biomedical, sensor, and environmental applications.[25] Biomimetic approaches have provided hydrogels that more closely replicate the extracellular matrix, presenting engineered physical, chemical, and biological cues to guide tissue regeneration processes.[26] Moreover, the development of conductive hydrogels, derived from intrinsically conducting polymers or functional composites, allows for applications in biosensors, tissue engineering of electro-responsive tissues, and flexible electronics.[27] Essential oil-based hydrogels are yet another functional type, delivering controlled antibacterial release and high biocompatibility for biomedical and food uses.[28] Additionally, advances in additive manufacturing and 3D bioprinting enable the fabrication of custom-shaped hydrogels, leveraging both natural and synthetic polymers, for the large-scale production of complex tissues and scaffolds.[29] As new anti-freezing hydrogels are created through network design and additive integration, their applications in cold environments extend to wearable sensors and soft robotics.[30] Finally, the development of cross-linking methods, from microwave-assisted synthesis to UV, further extends the diversity of hydrogel formulations, enabling novel combinations of injectability, structural strength, and biological activity, making them suitable for both medical and engineering applications.[31]

Polyampholyte and polyelectrolyte polymeric structures serve as highly effective adsorbents for the simultaneous removal of metal ions and dyes from wastewater due to their tunable chemical composition, pH-responsive behaviour, and abundant functional groups that enable both electrostatic complexation and chelation mechanisms.[32–34] The incorporation of imidazole rings and related triazole/pyrazole heterocycles into these polymeric backbones is crucial for enhanced performance, as the nitrogen-containing heterocycles with coordinating lone pairs form stable complexes with metal cations like Cu^{2+} and Hg^{2+} while the degree of aromatic substitution and structural modifications of these nitrogen heterocycles directly control the selectivity, binding strength, and overall adsorption capacity for both metal ions and anionic dyes through optimized steric and electronic effects.[35–37]

Ionic liquids (ILs) are an essential class of compounds that refer to salts that are molten at or near room temperature and have abnormal physicochemical characteristics such as low volatility, high thermal stability, solubility that can be tuned, and high ionic conductivity, which make them enormously helpful for a wide range of scientific and industrial applications.[38] Their development has moved in three main generations: first-generation ILs were introduced by Paul Walden in 1914 after the synthesis of ethylammonium nitrate. They were unstable but air and water-sensitive, limiting their practical sense. However, this was reversed in the 1990s with the introduction of second-generation ILs, which utilized weakly coordinating anions, thereby enhancing their stability and expanding their applications in catalysis, separation, and environmentally friendly solvents.[39] Third-generation 21st-century ILs have been designed with explicit functional applications, such as biodegradability and biocompatibility, becoming of enormous importance in pharmaceutical and biomedical applications.[40] Polymeric ionic liquids (PILs or polyILs) consist of polymeric backbones with IL moieties as repeating units, benefiting from the processability and flexibility of polymers and the thermal properties that can be tuned along with the ionic conductivity of ILs.[41] PILs and their copolymers have enabled the creation of sophisticated, highly performing materials that serve pivotal roles in applications such as chemical sensing, actuators, solid-state batteries, and nanotechnology.[42] Besides these, IL incorporation into polymer matrices has led to thermally stable, mechanically strong, and improved ion-conducting materials that allow for next-generation energy devices and green technologies.[43,44]

Research on the design and synthesis of novel poly(IL)s is imperatively targeted with the application of desired poly(IL)s driven by the basic characteristic properties of their polymerizable IL monomers. Specifically, poly(IL)s can be fine-tuned to exhibit either hydrophobic or hydrophilic behavior by selecting the appropriate counter anions. Many of our previous studies have targeted the design of polycationic (*i.e.*, polymer-bound cations, primarily imidazolium groups) and polyanionic (*i.e.*, polymer-bound anions, mainly delocalized sulfonimides) materials *via* UV-directed photopolymerization and have exclusively investigated their membrane applicability toward CO_2 separation.[45–47] With the success of fabricating self-standing defect-free membranes, the possibility of forming hydrogels from super-hydrophilic polymerizable ILs also becomes a reality.

In this study, we report the design and synthesis of imidazolium-mediated poly(IL) hydrogels having multifunctional applications, including high pollutant removal efficiency and enhanced drug adsorption. To achieve our goal, as depicted in Fig. 1, we have strategically developed a bisimidazole

Fig. 1 Schematic diagram for the preparation of the newly developed imidazolium-mediated poly(IL) hydrogel and its pollutant removal performance.

monomer $BImEG_3$ having three units of ethylene glycol (EG) chain as a spacer between two imidazole rings with a terminal vinyl group. Further interest turned out to be in the selection of more crosslinking network structures within this imidazolium poly(IL) matrix, whereby choosing an appropriate crosslinker, such as poly(ethylene glycol) diacrylate (PEGDA), may also enhance the overall performance of the resultant hydrogels. In the previous studies reported so far, the imidazolium moieties are utilized either as pendant side chains grafted into a polymeric backbone or they are attached with physically blended ionic liquid components, while the hydrogel reported here is distinguished by a bisimidazolium monomer crosslinked with PEGDA, resulting in the formation of a hydrogel with a uniformly distributed, structurally fixed ionic network, with high-density imidazolium sites that function as active crosslinking and adsorption centres. In this work, therefore, we anticipate a promising strategy for the introduction of quaternized imidazolium groups as active adsorption sites for anionic molecules such as azo dyes (*e.g.*, methyl orange, MO) and pharmaceutical products (*e.g.*, sodium diclofenac, DCl) together with PEG chains into the macrostructures of crosslinked hydrogels for achieving remarkable hydrophilicity in terms of unprecedented swelling properties.

2. Experimental section

2.1 Materials

N-Vinylimidazole (Sigma-Aldrich, 99%, M_W: 94.11), polyethylene glycol (PEGDA, M_W: 500, Sigma-Aldrich, 98%), 1,2-bis(2-bromoethoxy)ethane (TCI, 98%), acetone (Merck, 98%), *N*,*N*-dimethylformamide (DMF, Merck, 99%), methyl orange (MO, Sigma-Aldrich, 99%), diclofenac sodium salt (CIPLA), hexane (Sigma-Aldrich) and diethyl ether (Sigma-Aldrich, 99%) were purchased from the suppliers. All of these materials were used further without purification. Milli-Q water was used in all experiments.

2.2 Synthesis of 1,1′-((ethane-1,2-diylbis(oxy))bis(ethane-2,1-diyl))bis(3-vinyl-1*H*-imidazol-3-ium) bromide (BImIL, [BIMEG3])

1,2-Bis(2-bromoethoxy)ethane (3.05 g, 11.05 mmol) and 1-vinylimidazole (2 g, 21.25 mmol) were dissolved in acetone (20 mL). The mixture was stirred at 45 °C for 24 h, and then hexane (60 ml) was added to precipitate the resultant bis-vinylimidazolium bromide salt. The resultant compound was filtered and washed with hexane 3 times, and then dried under a vacuum oven overnight at 40 °C to give [$BIMEG_3$] (4.5 g). Yield: 88%. ^{1}H NMR (500 MHz, DMSO-d_6) δ: 9.41 (d, 2H), 8.19 (d, 2H), 7.86 (d, 2H), 7.34 (m, 2H), 5.96 (d, 2H), 5.45 (d,2H), 4.39 (t, 4H), 3.79 (d, 4H), 3.54 (m, 4H). The obtained NMR spectra are given in the SI (Fig. S1).

Table 1 Composition of the hydrogel solution used for the preparation of [$BIMEG_3$/PEGDA]-based membranes

Sample	[$BImEG_3$] (mg)	PEGDA (mg)	DMF
[$BImEG_3$/PEGDA] [10 : 90]	100	900	2.5 mL
[$BImEG_3$/PEGDA] [20 : 80]	200	800	2.5 mL
[$BImEG_3$/PEGDA] [30 : 70]	300	700	2.5 mL

2.3 Synthesis of [$BIMEG_3$]–PEGDA hydrogels

The newly designed imidazolium-mediated hydrogels were prepared using UV crosslinking of the as-synthesized polymerized bisimidazolium monomer ($BIMEG_3$) with a desired ratio of PEGDA crosslinker (10 : 90, 20 : 80, and 30 : 70, respectively, to $BIMEG_3$ and PEGDA). All the crosslinker compositions were dissolved in 2.5 ml of DMF together with a commercially available photoinitiator (2-hydroxy-2-methylpropiophenone). The amount used to prepare each hydrogel is listed in Table 1.

The resultant solution was allowed to degas and dissolve completely by ultrasonication for 10 minutes at room temperature. The polymerizable mixture was then poured onto a clean, Rain-X-coated quartz plate and sandwiched between two identical quartz plates on top with a spacer of aluminum tape to control the thickness of the hydrogels. The plates were then placed for a 30 minute photo-curing process under a 365 nm UV lamp (0.8 mW cm^{-2} at 4 cm distance). After irradiation, the plates were easily separated using a clean razor blade, thanks to the spacers. The crosslinked imidazolium-mediated hydrogel was then peeled off and immersed in 100 mL of water to remove excess DMF. This step was repeated twice to ensure the complete removal of water, and then the sample was kept in a vacuum oven overnight. The crosslinked membranes with different amounts of monomer and PEGDA were named

[$BImEG_3$/PEGDA] [10 : 90], [$BImEG_3$/PEGDA] [20 : 80], and [$BImEG_3$/PEGDA] [30 : 70].

2.3.1. Fourier-transform infrared (FT-IR) spectroscopy. Functional group analysis was performed on a Nicolet iS10 FT-IR spectrophotometer with 4000–400 cm^{-1} scan range and a resolution of 4 cm^{-1} accumulating 32 scans for each sample. A little amount of powder or a fragment of dried gel was pressed onto the diamond HATR crystal directly for analysis depending on the nature of the sample.

2.3.2. Proton nuclear magnetic resonance (^{1}H-NMR). ^{1}H NMR spectra were recorded on a Bruker Avance (500 MHz) instrument using deuterated dimethyl sulfoxide (DMSO-d_6) as a reference. For analysis, approximately 10 mg of every sample was dissolved in 500 μL DMSO-d_6 to obtain a clear solution, which was then transferred into an NMR tube for analysis.

2.3.3. Thermogravimetric analysis (TGA). Thermogravimetry was performed on a Netzsch DSC-TGA with IR coupling. The measurements of the TGA were performed in the temperature range of 30–900 °C with a heating rate of 10 °C min^{-1} and a flow of nitrogen at 20 mL min^{-1} to supply an inert atmosphere.

2.3.4. Ultraviolet-visible (UV-vis) spectroscopy. UV-visible spectrophotometric analyses were conducted using a Shimadzu UV-1900i UV-Visible spectrophotometer. For analysis, 2.5 mL of liquid sample was placed in a 3.5 mL quartz cuvette having a 1 cm optical path length, and spectra were recorded in the range of 250–700 nm wavelengths.

2.3.5. Energy dispersive X-ray (EDX) spectroscopy. The morphology and distribution of the sample composition was obtained from field-emission scanning electron microscopy (FE-SEM, Crossbeam 540, Carl Zeiss) with energy-dispersive X-ray spectroscopy (EDS). The measurements were made at an accelerating voltage of 20.0 kV, and the samples were directly placed in the microscope by placing small pieces of the gel in it without any additional treatment.

2.4 Swelling experiments

The swelling behaviour of hydrogels was investigated by immersing *ca.* 10 mg of dry PIL gel in 20 mL of water. The swollen specimens at discrete time intervals (2–20 min) were carefully transferred with a spatula, gently wiped with tissue paper to remove any water on the surface, and weighed immediately. The experiment was repeated three times in each set and continued until the swelling ratio (%SW) reached a stationary equilibrium value. The percentage of swelling calculated using eqn (1):

$$\%\mathrm{SW} = \frac{w_{\mathrm{wet}} - w_{\mathrm{dry}}}{w_{\mathrm{dry}}} \times 100 \quad (1)$$

where w_{wet} and w_{dry} represent the weights of the hydrated and dry samples, respectively.[3]

2.5 Gel fraction studies

The gel fraction of the crosslinked membranes was measured by immersing the prepared membranes in THF for 72 h. The extracted membranes were dried at 100 °C for 24 h, and the weights before and after extraction were measured to determine the gel fraction using the following equation:

$$\text{Gel fraction}\,\% = \frac{W_2}{W_1} \times 100$$

where W_1 and W_2 are the weights of the membrane before and after THF immersion, respectively.

2.6 Adsorption of the hydrogel with methyl orange and sodium diclofenac

The adsorption capacity of the gels toward pollutants was evaluated against methyl orange (MO) and sodium diclofenac as a model dye and drug compound, respectively. For kinetic experiments, 20 mg of dry adsorbent was immersed in 20 mL of 32 ppm methyl orange solution and 25 ppm sodium diclofenac solution. The concentration was measured every one hour by UV-visible spectroscopy and the respective adsorption capacity was calculated using the following equation:

$$q_t = \frac{(C_0 - C_t)V}{w} \quad (2)$$

where C_0 and C_t are the initial concentration and the concentration at time t, W, V and q correspond to the mass of the dry adsorbent used for the adsorption, the volume of the pollutant solution and the adsorption capacity of the prepared hydrogel in mg of pollutant per gram of the methyl orange. Maximum adsorption capacity was determined from pollutant solutions of various initial concentrations 30 to 150 ppm for methyl orange (MO) and 25 to 150 ppm for sodium diclofenac. The hydrogels were placed in the solutions and subjected to constant stirring conditions at 300 rpm for 12 hours for equilibrium achievement. The adsorption equilibrium q_e was calculated through eqn (3), using the equilibrium concentration (C_e) of the dye or drug remaining in solution, the data were fitted to the Langmuir adsorption isotherm model equation and the theoretical adsorption maximum was calculated using eqn (4). The concentrations of MO and diclofenac were evaluated by monitoring the adsorption maxima of both the pollutants at 465 and 275, respectively.

$$q_e = \frac{(C_0 - C_e)V}{w} \quad (3)$$

$$\frac{C_e}{q_e} = \frac{1}{q_{\max} K_L} + \frac{C_e}{q_{\max}} \quad (4)$$

2.7 Batch adsorption kinetics

For the determination of the adsorbed mercury on the hydrogel matrix, experiments were done in a mercury analyzer (model MA-3000, Nippon Instruments, North America). 30 mg of the hydrogel was used as an adsorbing material. The % of Hg removal and adsorption capacity were calculated as given in the following equation:

$$\text{Mercury removal}\,(\%) = \frac{(C_0 - C_f)}{C_0} \times 100 \quad (5)$$

$$\text{Adsorption capacity } (q) = (C_0 - C_t) \times \frac{V}{m} \quad (6)$$

where, C_0 is the Hg initial concentration (ppm), C_f is the Hg concentration at the experiment end (ppm), C_t is the Hg concentration at time t (ppm), V is the solution volume (L), and m is the mass of [$BImEG_3$/PEGDA] (mg).

2.8 X-ray photoelectron spectroscopy (XPS)

The surface elemental composition of the modified kaolin was investigated before and after adsorption through X-ray photoelectron spectroscopy (XPS) using a NEXSA XPS system (Thermo Scientific, Waltham, MA, USA). The measurement was done by irradiating the sample with a micro-focused, monochromated Al K-alpha X-ray beam with the photon energy approximately equal to 1486.6 eV.

3. Results and discussion

As outlined in Scheme 1, the synthesis of a polymerizable bisimidazolium monomer, $BImEG_3$, featuring three ethylene glycol (EG) units as spacers between two imidazole rings with a terminal vinyl group, was conducted *via* a Menshutkin reaction, as previously reported in our work.[48] The purity and structure of the newly synthesized $BImEG_3$ monomer were qualitatively confirmed by spectroscopic measurements, including ^{1}H NMR (see SI Fig. S1) and FTIR (Fig. 2). The selection of a technique for high-performance hydrogel fabrication always depends on the choice of the crosslinker for the desired applications. Our further interest focused on the selection of more crosslinked network structures, wherein the selection of an appropriate crosslinker, poly(ethylene glycol) diacrylate (PEGDA), supports the newly developed imidazolium poly(IL) matrix. Therefore, in this work, a weight equivalent ratio was considered to generate an imidazolium-mediated crosslinked network within PEGDA substructures *via* the UV-photopolymerization method, as depicted in Scheme 1. As such, various weight ratios of monomer ($BImEG_3$) and crosslinker (PEGDA) of 10 : 90, 20 : 80, and 30 : 70, repetitively, were targeted to yield the corresponding compositions of hydrogels, [$BImEG_3$/PEGDA] [10 : 90], [$BImEG_3$/PEGDA] [20 : 80], and [$BImEG_3$/PEGDA] [30 : 70]. Each of the $BImEG_3$/PEGDA hydrogels formed flexible, free-standing hydrogels, a desirable characteristic for adsorption and removal studies. The formation of the newly developed imidazolium-mediated poly(IL) hydrogels was confirmed by FTIR spectroscopy.

As depicted in Fig. 2, the functional group identification and extent of crosslinking were confirmed by FT-IR spectra. The result revealed that the characteristic peaks corresponding to the C=C stretching (at 1640 cm^{-1}) and =CH_2 bending (at 920 and 790 cm^{-1}) of the vinyl groups in the [$BIMEG_3$] monomer disappeared after UV-irradiation, indicating complete crosslinking of the polymer network to form hydrogels.[47] At the same time, the existence of peaks at 1465 cm^{-1} corresponds to the aromatic C=C stretching frequency of the imidazolium cation, confirming that the ionic side groups from the

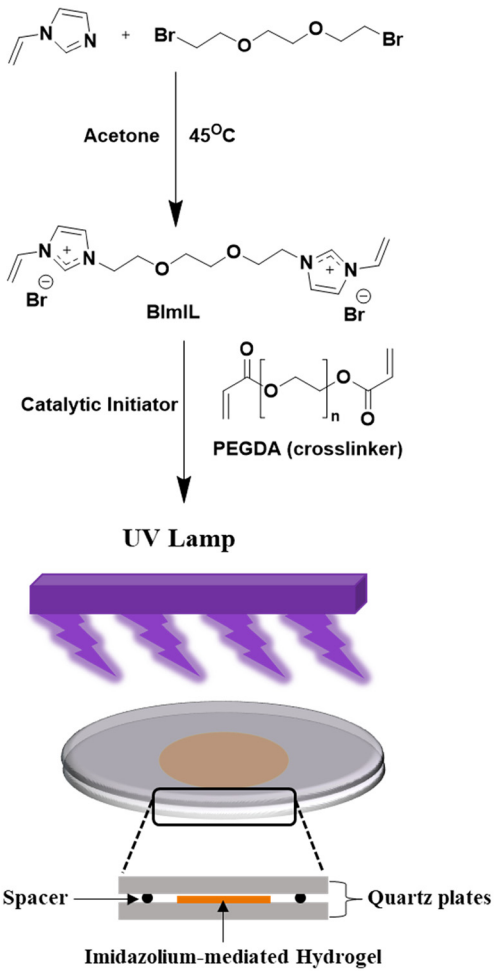

Scheme 1 Synthetic route to obtain a bisimidazolium-mediated polymerizable monomer, BImIL, and schematic representation of UV crosslinking to yield a $BImEG_3$/PEGDA hydrogel.

monomer are incorporated successfully into the hydrogel.[4] In addition, the band observed between 2860 and 3000 cm^{-1} is attributed to the characteristic absorption of the aliphatic CH_2 group in the material.

TGA analysis of the newly developed imidazolium-mediated poly(IL) further assessed the stability and the effect of crosslinking on the generation of a stable hydrogel, which is desired for use in adsorption capacity and separation performance. Interestingly, all the hydrogel compositions exhibited similar thermograms, displaying two-stage degradations with thermal stabilities of up to 280 °C, as shown in Fig. 3. While the first stage of weight loss occurs between 280 and 380 °C, which is attributed to the decomposition of the PEGDA crosslinker and the vinyl radical-generated crosslinked part of the cationic imidazolium groups in the polymer backbone, the second shoulder degradation between 340 °C and 450 °C is attributed to the decomposition of the anions and imidazole ring, as observed in other PIL matrices reported elsewhere.[49] Overall, the TGA revealed that all the imidazolium-mediated poly(IL) hydrogel compositions are sufficiently stable and

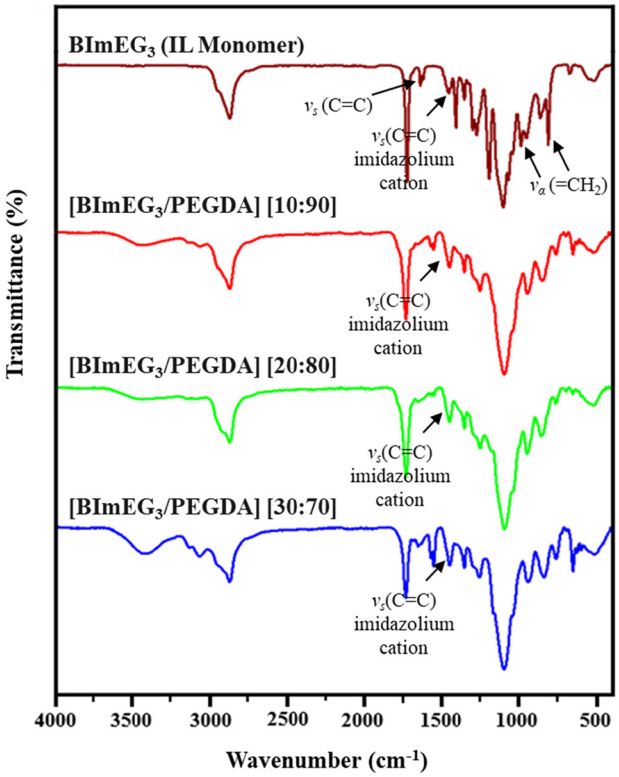

Fig. 2 (a) FT-IR spectra of the starting materials and hydrogels with different $BIMEG_3$: PEGDA ratios.

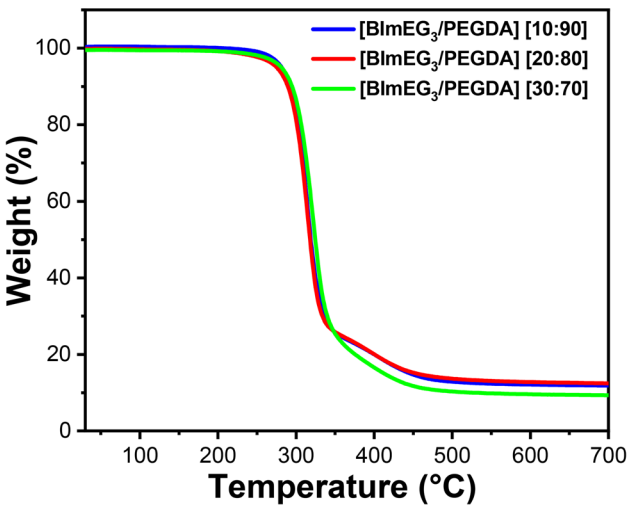

Fig. 3 TGA thermograms of the newly developed imidazolium-mediated poly(IL) hydrogels.

capable of removing pollutants and/or anionic dyes under elevated temperature conditions.

The morphology of the newly developed imidazolium-mediated hydrogels was investigated using scanning electron microscopy (SEM), with cross-sectional images of the samples (Fig. 4). Interestingly, the novel [$BIMEG_3$]/PEGDA hydrogels exhibited a cross-sectional surface with an interconnected network structure with precisely formed pores of variable shape and size, consistent with the results observed by Buldain and co-workers.[50] In addition, the rough surface of interconnected hydrogels indicates a pivotal key feature of possible hydrogel function, such as extraordinary swelling behavior and enhanced adsorption/removal capacity toward small molecules, including anionic dyes and metal ions.[51] A comprehensive study of mercury removal and anionic dye adsorption is presented in the following sections. In an additional investigation of morphological analysis, FE-SEM further confirmed the micro-substructural components of the newly developed [$BIMEG_3$]/PEGDA hydrogels *via* the presence of bromine anions as a "free" counterion of cationic backbones of imidazolium groups in the polymeric network, as depicted in Fig. 5.

All the freshly synthesized imidazolium-mediated poly(IL) hydrogel was systematically studied for their swelling property calculations. To this point, all the hydrogels were shaped to the same size; the samples were immersed in Milli-Q water and weighed at specific time intervals until they reached equilibrium. Fig. 6a illustrates the swelling properties of the hydrogels with varying cross-linking ratios ([$BImEG_3$/PEGDA] [10 : 90], [$BImEG_3$/PEGDA] [20 : 80], and [$BImEG_3$/PEGDA] [30 : 70]) and a model hydrogel [$BImEG_3$/PEGDA] [0 : 100] without a vinylimidazolium monomer. It was noteworthy that all the samples except for the model hydrogel [$BImEG_3$/PEGDA] [0 : 100] exhibited a swelling ratio of more than 200% and continued to increase to a maximum of 235% after 2 hours of immersion. It is already evident from the reported literature that the water swelling capacity of hydrophilic PEG-containing hydrogels significantly contributes to an enhanced swelling ratio. In this study, a similar observation was found with a high swelling rate of 235% for the optimum Bim IL *vs.* PEGDA crosslinker combination, [$BImEG_3$/PEGDA] [30 : 70]. The model hydrogel [$BImEG_3$/PEGDA] [0 : 100] shows a swelling capacity of 80% after two hours of immersion. To understand the stability of the prepared membrane, the swelling experiments were repeated after the samples were dried in a vacuum oven at 60 °C for 24 hours. The hydrogels were re-immersed in water, and the experiments were repeated. As such, the swelling kinetics for all three compositions of imidazolium-mediated hydrogels were studied for three cycles. The results indicated that the gel membranes exhibited excellent stability in their swelling properties, with nearly the same swelling capacities for three consecutive cycles (Fig. 6b). A mean swelling ratio of 230.0 ± 2.2% was achieved, indicating that water immersion did not lead to degradation or dissolution. This is a testament to the success of cross-linking between the two polymers, which locked in the structural integrity of the hydrogels and foresees the best performance toward adsorption applications.

The gel fraction studies, which provide a quantitative measure of crosslinking density and the material's structural integrity, were obtained by measuring the mass fraction of the undissolved polymer remaining after the hydrogel was soaked

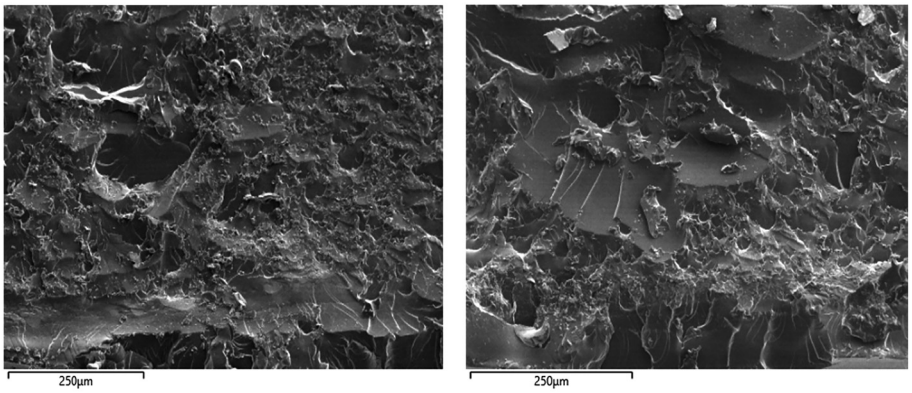

Fig. 4 Cross-sectional SEM images of the newly developed imidazolium-mediated poly(IL) hydrogels having a high loading of BImIL: (a) [$BIMEG_3$/PEGDA] [20 : 80] and (b) [$BIMEG_3$/PEGDA] [30 : 90].

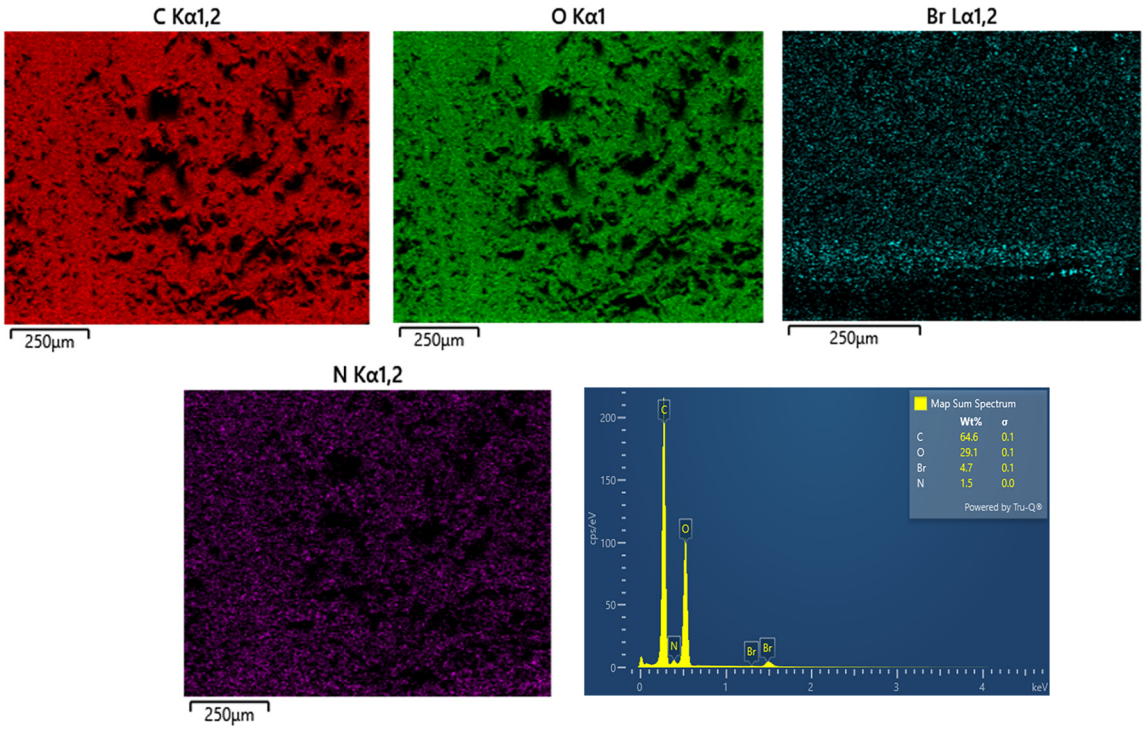

Fig. 5 EDX analysis of imidazolium-mediated poly(IL) hydrogels with the most loaded monomer, [$BIMEG_3$/PEGDA] [30 : 90].

in THF for 2 days. The calculated gel fraction was above 98% for all three newly developed imidazolium-mediated hydrogels, indicating the effective crosslinking network in the hydrogel matrices (Table 2). The gel fractions of the membranes showed little-to-no change upon continuous soaking in THF for 15 days, indicating high chemical stability or high ionic strength without any leakage of IL units formed in the crosslinked PIL substructures.

Furthermore, the newly developed imidazolium-mediated poly(IL) hydrogel material, having the highest loading of the BImIL monomer and exhibiting good swelling performance, [$BImEG_3$/PEGDA] [30 : 70], was further targeted as an optimum combination and investigated as an adsorbent for model anionic pollutants, such as diclofenac (DlC) and methyl orange (MO), in water. In general, the adsorption mechanism of anionic pollutants in hydrogels can be fine-tuned by generating a hydrogel with high swelling capacity and incorporating ionic functionality into the crosslinked hydrogel matrix. Interestingly, in this study, we have exclusively targeted a synergetic effect by combining the benefits of PEG chain units, which provide high swelling efficiency, while the imidazolium moieties contribute to higher electrostatic interactions with

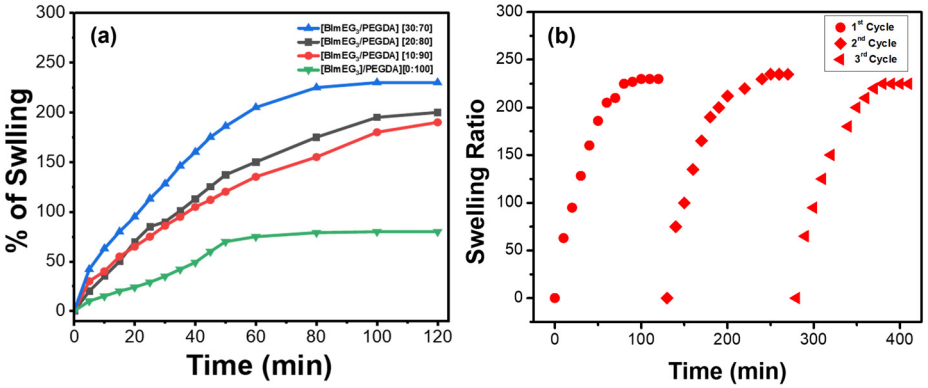

Fig. 6 Swelling kinetics of all three newly developed imidazolium-mediated poly(IL) hydrogels and the zero-loaded IL crosslinker hydrogel having a pure PEGDA matrix at room temperature (a) and recyclability of the hydrogel [BImEG$_3$/PEGDA] [30 : 70] (b).

Table 2 Gel fraction studies of the hydrogels soaked in THF for up to 5 days

Samples	Gel fraction% 2 days	10 days
[BImEG$_3$/PEGDA] [10 : 90]	98.2	97.1
[BImEG$_3$/PEGDA] [20 : 80]	98.1	96.3
[BImEG$_3$/PEGDA] [30 : 70]	98.5	96.9

anionic substances, thereby increasing the overall efficiency of the newly developed imidazolium-mediated poly(IL) hydrogel as an adsorbent.

As depicted in Fig. 7, the [BImEG$_3$/PEGDA] [30 : 70] hydrogel was able to adsorb approximately 90% of the MO and 89% of the diclofenac dye within 24 hours and successfully cleaned the pollutant after 36 hours (Fig. S4 and S5). To better understand the adsorption capacity of the newly developed imidazolium-mediated poly(IL) hydrogel, Langmuir adsorption isotherms were plotted with the [BImEG$_3$/PEGDA] [30 : 70] sample. The plot shows a good fit, with R^2 values of 0.999 and 0.995, respectively. The maximum adsorption capacity (q_{max}) was calculated by taking the reciprocal of the slope of the plot. The equilibrium adsorption capacities were found to be 158.73 mg g^{-1} and 127.22 mg g^{-1} for methyl orange and diclofenac dyes, respectively, which are comparable to those reported for other polymeric materials in the literature, as provided in Table 3. Interestingly, the material is highly efficient when compared with other systems reported such as natural materials derived from chitosan,[52,53] cellulose,[54] aliginate/carbon based films[55] and the natural product extract of *Guazuma ulmifolia* Lam. fruit.[56] The hydrogel also performed better than the polyaniline-based synthetic polymer reported by Haitham *et al.*[57] in 2019.

On the other hand, heavy metal toxicity remains a primary environmental concern because its persistence and bioaccumulation pose severe health risks to both aquatic and terrestrial organisms, particularly mercury (Hg) content, which causes severe damage even at the ppm level. Contamination of Hg in the aquatic ecosystem can even return to the human body through the food chain *via* water and fish. Thus, the development of low-cost materials to remove mercury from water, air, and industrial effluents is a significant concern for researchers worldwide. Polymeric hydrogels have emerged as highly effective adsorbents for mercury ions due to their three-dimensional porous network structure, high water retention capacity, and abundant functional groups that facilitate metal–ligand interactions. As such, the performance of the newly developed imidazolium-mediated poly (IL) hydrogels for mercury adsorption was measured in batch mode by bringing 30 mg of the adsorbent samples into contact with 50 ppm mercury ($HgCl_2$) solutions.

The adsorption kinetics studies revealed that imidazolium-mediated poly(IL) hydrogels reached equilibrium removal efficiencies of nearly 90%, 75%, and 66% in 12 h for [BImEG$_3$/PEGDA] [30 : 70], [BImEG$_3$/PEGDA] [20 : 80], and [BImEG$_3$/PEGDA] [10 : 90] with adsorption capacities of 217.5 mg g^{-1}, 178.5 mg g^{-1}, and 160 mg g^{-1}, respectively (Fig. 8). The higher adsorption capacity for the combination of [BImEG$_3$/PEGDA] [30 : 70] was plausibly due to the higher ratio of the crosslinked imidazolium groups having "free" counter anions.[66] More specifically, the incorporation of imidazolium groups as a key functional monomer in this hydrogel matrix enhances Hg intake by serving as coordination sites for mercury ions. It is also evident that imidazole-based ionic liquids have demonstrated excellent chelating affinity and selective adsorption capabilities toward heavy metals.[67] Whereas crosslinked PEG chains helped to form the structural stability of the hydrogel, keeping appropriate swelling properties.[68,69] These results suggest that an optimized polymer ratio, which balances structural integrity and the availability of active binding sites, is necessary for successful Hg capture. It is noteworthy that an equilibrium removal efficiency of 99% was achieved by all three imidazolium-mediated poly(IL) hydrogels within 24 hours, indicating that the newly developed hydrogel materials exhibit significant adsorption capacity and kinetics, making them strong candidates as adsorbents for purifying Hg-contaminated water.

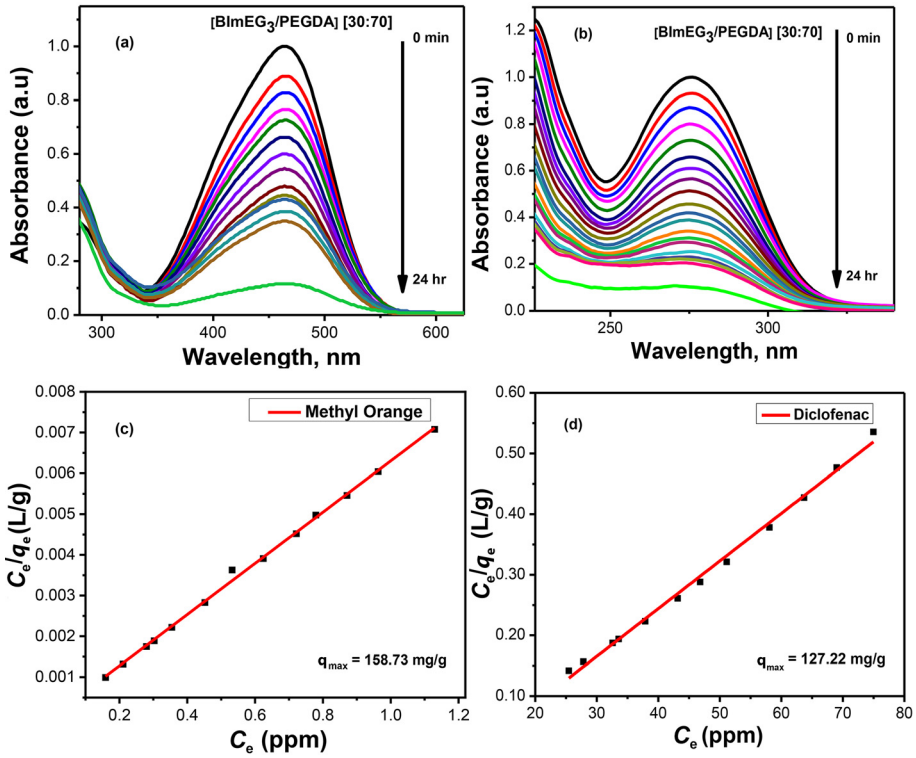

Fig. 7 UV-Visible absorption spectra of methyl orange and diclofenac (a and b). Langmuir adsorption isotherm of the methyl orange and diclofenac solution adsorbed on the [BImEG$_3$/PEGDA] [30 : 70] matrix (c and d).

Table 3 Comparison of the adsorption capacity of various materials reported so far towards methyl orange and diclofenac dyes

Methyl orange				Diclofenac			
Adsorbent	q_{max} (mg g^{-1})	pH value	Ref.	Adsorbent	q_{max} (mg g^{-1})	pH value	Ref.
UiO-66 MOF	454.0	12.0	58	Cellulose based aerogel	605.8	7.1	59
N-Acyl thiolated chitosan	434.9	7.0	60	PAA/NC hydrogel	559.8	4.0	61
PIM-1	312.5	7.0	62	UiO-66-NH$_2$ (90)	555.0	5.6	63
P4VP : PEG PIL	218.8	7.0	3	Magnetic cellulose ionomer	268.0	9.0	64
Protonated cross-linked chitosan	180.2	4.5	65	P4VP : PEG PIL	166.7	7.0	3
Polyaniline powder	147.0	7.0	51	Chitosan grafted adsorbent	84.6	4.0	46
Chitosan beads	73.0	3.0	47	Alginate/carbon-based films	29.9	3.0	49
Cellulose derived from *Stipa tenacissima* L.	16.9	3.7	48	*Guazuma ulmifolia* Lam. fruit	27.8	6.0	50
[BImEG$_3$/PEGDA] [30 : 70]	158.73	7.0	This work	[BImEG$_3$/PEGDA] [30 : 70]	127.22	7.0	This work

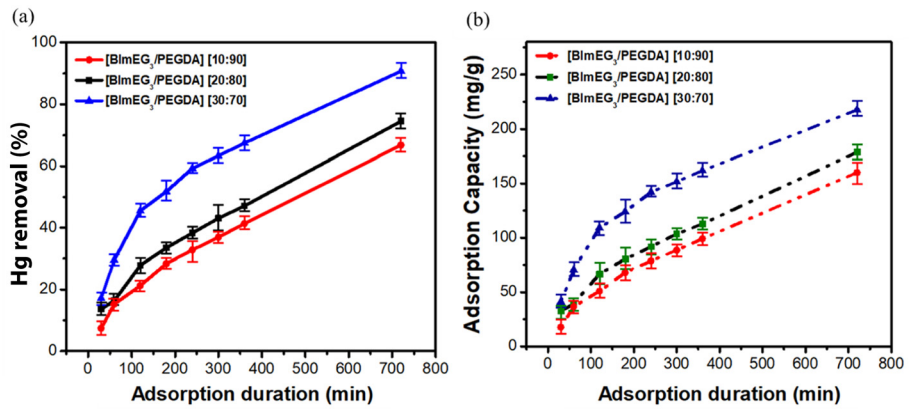

Fig. 8 Hg^{2+} removal efficiency of the newly developed imidazolium-mediated poly(IL) hydrogels (a) and their Hg^{2+} adsorption capacity (b).

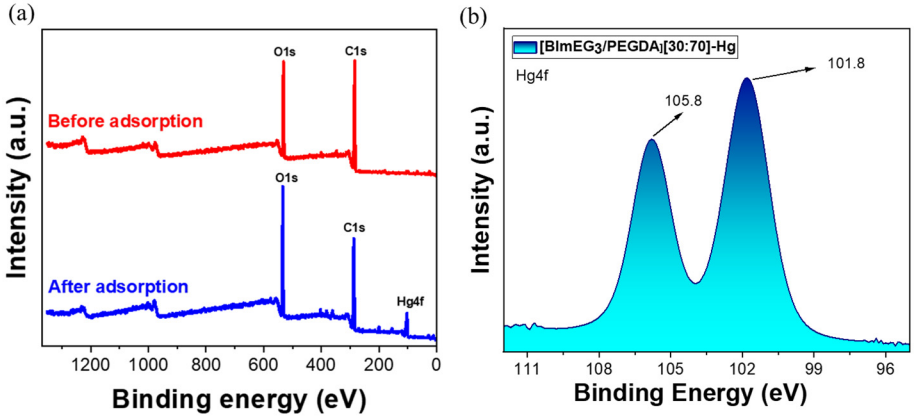

Fig. 9 XPS survey spectra. (a) XPS spectrum of Hg4f in [BImEG$_3$/PEGDA] [30 : 70] after adsorption (b).

To obtain a clear idea of the potential mechanism of Hg^{2+} adsorption, the newly developed imidazolium-mediated poly (IL) hydrogel material, [BImEG3/PEGDA] [30 : 70], which has the highest loading of the BImIL monomer and exhibits good swelling performance, was further analysed using XPS. Fig. 9a displays the XPS survey spectra of the [BImEG$_3$/PEGDA] [30 : 70] material, before and after the adsorption of Hg^{2+}. The peaks of C 1s, O 1s, N 1s, Cl 2p, and Br 3d were observed in [BImEG$_3$/PEGDA] [30 : 70] while after adsorption of metal ions, the peak of Hg 4f was observed in the XPS spectra of [BImEG$_3$/PEGDA] [30 : 70]-Hg(II), suggesting that Hg^{2+} was adsorbed on [BImEG$_3$/PEGDA] [30 : 70]-Hg(II) successfully. Furthermore, the high-resolution XPS spectrum of Hg 4f in [BImEG$_3$/PEGDA] [30 : 70] after adsorption showed two strong Hg $4f_{5/2}$ and Hg $4f_{7/2}$ peaks at 105.8 and 101.8 eV, respectively, indicating that Hg^{2+} was adsorbed on the material within a divalent mode.[70,71]

4. Conclusion

We have successfully designed and synthesized a highly tunable and multifunctional imidazolium-mediated poly(IL) hydrogel *via* the photopolymerization of a bisimidazole monomer featuring three units of ethylene glycol (EG) chains as spacers between two imidazole rings with an appropriate cross-linker, PEGDA. Structural characterization by FT-IR, TGA, and SEM confirmed the formation of a well-defined cross-linked network, while swelling and adsorption analyses demonstrated the strong influence of imidazolium loading on the physicochemical properties of the hydrogels. Among the newly developed imidazolium-mediated hydrogels, the optimized composition of [BImEG$_3$/PEGDA] [30 : 70] exhibited outstanding adsorption capacity towards industrial and pharmaceutical dyes such as methyl orange and diclofenac, with q_{max} values of 156.73 mg g^{-1} and 127.22 mg g^{-1}, respectively. In addition, the newly developed imidazolium-mediated poly(IL) hydrogel demonstrated a complete removal efficiency of ~99% within 24 hours for Hg^{2+} ions, with a superior adsorption capacity of 217.5 mg g^{-1} for the combination of [BImEG$_3$/PEGDA] [30 : 70] after 12 hours, indicating its potential for Hg^{2+} removal from water. In summary, the high swelling capacity, strong electrostatic interaction, and unique structural features suggest that the newly developed imidazolium-mediated poly(IL) hydrogel is a unique, multifunctional material, making it a strong candidate for wastewater treatment. Precisely, these hydrogels use a synergistic mechanism, such as electrostatic interactions, coordination bonding with metal ions, and hydrogen-bonding interactions introduced by bisimidazolium cations crosslinked within the PEG chain units, for adsorption processes *via* a feasible synthetic strategy of UV crosslinking. Interestingly, a comparably good DCI adsorption capacity leads to an extension study of these hydrogel materials as drug delivery systems, which will be the focus of our future work.

Conflicts of interest

The authors declare no conflicts of interest.

Data availability

The data supporting this article have been included as part of the supplementary information (SI). Supplementary information: Fig. S1 shows the NMR spectrum of the newly developed crosslinker ([BIMEG3]), and Fig. S2, S3, S4, and S5 show the calibration curves and adsorption kinetics of diclofenac and methyl orange, respectively. See DOI: https://doi.org/10.1039/d5lp00361j.

Acknowledgements

This research was funded by the Ministry of Science and Higher Education of the Republic of Kazakhstan (Grant No. AP26198095) and Nazarbayev University, through the Collaborative Research Project Grant (Grant No.

111024CRP2017) and the Faculty Development Competitive Research Grants Program (Grant No. 040225FD4729).

References

1 N. W. Wilson and G. G. Botte, Novel biopolymer pectin-based hydrogel electrolytes for sustainable energy storage, *Mater. Adv.*, 2024, **5**, 7312–7326.
2 Y. Taoka and K. Matsumura, Organic solvent-free gelation of syndiotactic-rich poly(vinyl alcohol), *RSC Appl. Polym.*, 2025, **3**, 1385–1392.
3 O. Ramírez, S. Castillo, S. Bonardd, C. Saldías, D. Díaz Díaz and A. Leiva, Poly(ionic liquid)-Based Hydrogel for Emerging Pollutant Removal and Controlled Drug Delivery, *ACS Appl. Polym. Mater.*, 2024, **6**, 13865–13876.
4 P. Haripriya and K. Vijayakrishna, A multifaceted poly(ionic liquid)-based superabsorbent hydrogel for simultaneous removal of heavy metals and synthetic dyes, *Polym. Chem.*, 2025, **16**, 3875–3885.
5 J. Mitrovic, G. Richey, S. Kim and M. O. Guler, Peptide Hydrogels and Nanostructures Controlling Biological Machinery, *Langmuir*, 2023, **39**, 11935–11945.
6 M. A. Cejas, W. A. Kinney, C. Chen, G. C. Leo, B. A. Tounge, J. G. Vinter, P. P. Joshi and B. E. Maryanoff, Collagen-Related Peptides: Self-Assembly of Short, Single Strands into a Functional Biomaterial of Micrometer Scale, *J. Am. Chem. Soc.*, 2007, **129**, 2202–2203.
7 A. M. Jonker, D. W. P. M. Löwik and J. C. M. Van Hest, Peptide- and Protein-Based Hydrogels, *Chem. Mater.*, 2012, **24**, 759–773.
8 F. Ding, S. Wu, S. Wang, Y. Xiong, Y. Li, B. Li, H. Deng, Y. Du, L. Xiao and X. Shi, A dynamic and self-crosslinked polysaccharide hydrogel with autonomous self-healing ability, *Soft Matter*, 2015, **11**, 3971–3976.
9 Y. Ke, K. Lan, J. Y. Wong, H. Lu, S. Gao, K. Ryu, F. Chen, W. W. Loh, Z. Dong, J. Y. C. Lim, Z. Dong, X. Chen, I. Willner and Y. Hu, Sustainable DNA-polysaccharide hydrogels as recyclable bioplastics, *Nat. Commun.*, 2025, **16**, 7467.
10 J. T. Chung, C. M. L. Lau and Y. Chau, The effect of polysaccharide-based hydrogels on the response of antigen-presenting cell lines to immunomodulators, *Biomater. Sci.*, 2021, **9**, 6542–6554.
11 S. Khodami, K. Kaniewska, J. Romanski, M. Karbarz and Z. Stojek, Amino Acid-Based Hydrogel with Interpenetrating Gelatin and Cross-Linked by Metal Ions, Providing High Stretchability and Motion Sensitivity, *ACS Omega*, 2025, **10**, 12062–12075.
12 A. Roy, K. Manna, S. Dey, K. Chakraborty, S. Dhara and S. Pal, Functionalized amino acid-based injectable hydrogels for sustained drug delivery, *Soft Matter*, 2025, **21**, 2836–2848.
13 E. R. Draper, K. L. Morris, M. A. Little, J. Raeburn, C. Colquhoun, E. R. Cross, T. O. McDonald, L. C. Serpell and D. J. Adams, Hydrogels formed from Fmoc amino acids, *CrystEngComm*, 2015, **17**, 8047–8057.
14 F. Huang, M. Chen, Z. Zhou, R. Duan, F. Xia and I. Willner, Spatiotemporal patterning of photoresponsive DNA-based hydrogels to tune local cell responses, *Nat. Commun.*, 2021, **12**, 2364.
15 Q. Chai, Y. Jiao and X. Yu, Hydrogels for Biomedical Applications: Their Characteristics and the Mechanisms behind Them, *Gels*, 2017, **3**, 6.
16 X. Ding, L. Fan, L. Wang, M. Zhou, Y. Wang and Y. Zhao, Designing self-healing hydrogels for biomedical applications, *Mater. Horiz.*, 2023, **10**, 3929–3947.
17 X. Le, W. Lu, J. Zhang and T. Chen, Recent Progress in Biomimetic Anisotropic Hydrogel Actuators, *Adv. Sci.*, 2019, **6**, 1801584.
18 A. K. Gaharwar, N. A. Peppas and A. Khademhosseini, Nanocomposite hydrogels for biomedical applications, *Biotechnol. Bioeng.*, 2014, **111**, 441–453.
19 Y. Lin, A. Wu, Y. Zhang, H. Duan, P. Zhu and Y. Mao, Recent progress of nanomaterials-based composite hydrogel sensors for human–machine interactions, *Discov. Nano*, 2025, **20**, 60.
20 G. H. D. Agbna and S. J. Zaidi, Hydrogel Performance in Boosting Plant Resilience to Water Stress—A Review, *Gels*, 2025, **11**, 276.
21 M. Neumann, G. D. Marco, D. Iudin, M. Viola, C. F. Van Nostrum, B. G. P. Van Ravensteijn and T. Vermonden, Stimuli-Responsive Hydrogels: The Dynamic Smart Biomaterials of Tomorrow, *Macromolecules*, 2023, **56**, 8377–8392.
22 P. Wang, Q. Liao and H. Zhang, Polysaccharide-Based Double-Network Hydrogels: Polysaccharide Effect, Strengthening Mechanisms, and Applications, *Biomacromolecules*, 2023, **24**, 5479–5510.
23 B. Wu, Y. Jian, X. Le, H. Lin, S. Wei, W. Lu, J. Zhang, A. Zhang, C.-F. Huang and T. Chen, Supramolecular Fabrication of Complex 3D Hollow Polymeric Hydrogels with Shape and Function Diversity, *ACS Appl. Mater. Interfaces*, 2019, **11**, 48564–48573.
24 A. J. R. Amaral and G. Pasparakis, Stimuli responsive self-healing polymers: gels, elastomers and membranes, *Polym. Chem.*, 2017, **8**, 6464–6484.
25 D. M. Alshangiti, T. K. El-damhougy, A. Zaher, M. Madani and M. Mohamady Ghobashy, Revolutionizing biomedicine: advancements, applications, and prospects of nanocomposite macromolecular carbohydrate-based hydrogel biomaterials: a review, *RSC Adv.*, 2023, **13**, 35251–35291.
26 K. D. Ngadimin, A. Stokes, P. Gentile and A. M. Ferreira, Biomimetic hydrogels designed for cartilage tissue engineering, *Biomater. Sci.*, 2021, **9**, 4246–4259.
27 N. K and C. S. Rout, Conducting polymers: a comprehensive review on recent advances in synthesis, properties and applications, *RSC Adv.*, 2021, **11**, 5659–5697.
28 M. Chelu, Hydrogels with Essential Oils: Recent Advances in Designs and Applications, *Gels*, 2024, **10**, 636.

29 M. Kandasamy, K. Vijayananth, A. Parasuraman and N. Ayrilmis, 3D Bioprinting of Biomaterials: A Review of Advances in Techniques, Materials, and Applications, *Polym. Adv. Technol.*, 2025, **36**, e70324.
30 D. Zhang, H. Chen, Y. Zhang, J. Yang, Q. Chen, J. Wu, Y. Liu, C. Zhao, Y. Tang and J. Zheng, Antifreezing hydrogels: from mechanisms and strategies to applications, *Chem. Soc. Rev.*, 2025, **54**, 5292–5341.
31 M. Y. Lee, E. S. Lee, N. Y. Ko, H. J. Kim, D.-H. Kim, G. D. Cha and J. H. Koo, Emerging roles of hydrogels, organogels, and their hybrids in soft bioelectronics and bioplatforms, *npj Biosens.*, 2025, **2**, 35.
32 K. Maity, S. Sau and S. K. Samanta, Post–Functionalization of Fluorinated Dibenzosulfone–Based Conjugated Polymer for Smart 'Turn–off' Sensing of Cu^{2+} Ions, *Chem. – Asian J.*, 2025, **20**, e202401053.
33 V. V. Annenkov, E. N. Danilovtseva, V. V. Saraev and A. I. Mikhaleva, Complexation of copper(II) ions with imidazole–carboxylic polymeric systems, *J. Polym. Sci. A Polym. Chem.*, 2003, **41**, 2256–2263.
34 E. N. Danilovtseva, M. A. Chafeev and V. V. Annenkov, New polyelectrolytes based on 4-vinyl–1,2,3-triazole and 1-vinylimidazole, *J. Polym. Sci. A Polym. Chem.*, 2012, **50**, 1539–1546.
35 D. Khaki, H. Namazi and S. M. Amininasab, Design and fabrication of photoactive imidazole-based poly(ether-imide)s and a polyimide/HBP-modified SiO_2 composite: toward high heat-resistance, antimicrobial activity and removal of heavy metal ions, *RSC Adv.*, 2021, **11**, 23574–23588.
36 M. Cortes-Clerget, J. Yu, J. R. A. Kincaid, P. Walde, F. Gallou and B. H. Lipshutz, Water as the reaction medium in organic chemistry: from our worst enemy to our best friend, *Chem. Sci.*, 2021, **12**, 4237–4266.
37 E. N. Danilovtseva, M. A. Chafeev and V. V. Annenkov, New polyelectrolytes based on 4-vinyl–1,2,3-triazole and 1-vinylimidazole, *J. Polym. Sci. A Polym. Chem.*, 2012, **50**, 1539–1546.
38 R. Ferraz, L. C. Branco, C. Prudêncio, J. P. Noronha and Ž Petrovski, Ionic Liquids as Active Pharmaceutical Ingredients, *ChemMedChem*, 2011, **6**, 975–985.
39 Y. Hu, Y. Xing, H. Yue, T. Chen, Y. Diao, W. Wei and S. Zhang, Ionic liquids revolutionizing biomedicine: recent advances and emerging opportunities, *Chem. Soc. Rev.*, 2023, **52**, 7262–7293.
40 N. Adawiyah, M. Moniruzzaman, S. Hawatulaila and M. Goto, Ionic liquids as a potential tool for drug delivery systems, *MedChemComm*, 2016, **7**, 1881–1897.
41 S.-Y. Zhang, Q. Zhuang, M. Zhang, H. Wang, Z. Gao, J.-K. Sun and J. Yuan, Poly(ionic liquid) composites, *Chem. Soc. Rev.*, 2020, **49**, 1726–1755.
42 D. M. Correia, L. C. Fernandes, P. M. Martins, C. García-Astrain, C. M. Costa, J. Reguera and S. Lanceros-Méndez, Ionic Liquid–Polymer Composites: A New Platform for Multifunctional Applications, *Adv. Funct. Mater.*, 2020, **30**, 1909736.
43 I. Kammakakam, K. E. O'Harra, G. P. Dennis, E. M. Jackson and J. E. Bara, Self–healing imidazolium–based ionene–polyamide membranes: an experimental study on physical and gas transport properties, *Polym. Int.*, 2019, **68**, 1123–1129.
44 A. Saddeeq, M. Mahmoudi Kouhi and I. Kammakakam, Advances of Ionic-Mediated Polymer Architectures for CO_2 Gas Separation Membranes: A Comprehensive Review of Design, Progress, and Future Prospects, *ACS Omega*, 2025, **10**, 26266–26292.
45 I. Kammakakam, J. E. Bara, E. M. Jackson, J. Lertxundi, D. Mecerreyes and L. C. Tomé, Tailored CO_2 -Philic Anionic Poly(ionic liquid) Composite Membranes: Synthesis, Characterization, and Gas Transport Properties, *ACS Sustainable Chem. Eng.*, 2020, **8**, 5954–5965.
46 I. Kammakakam, J. E. Bara and E. M. Jackson, Dual Anion–Cation Crosslinked Poly(ionic liquid) Composite Membranes for Enhanced CO_2 Separation, *ACS Appl. Polym. Mater.*, 2020, **2**, 5067–5076.
47 I. Kammakakam, A. H. N. Rao, H. W. Yoon, S. Nam, H. B. Park and T.-H. Kim, An imidazolium-based ionene blended with crosslinked PEO as a novel polymer membrane for selective CO2 separation, *Macromol. Res.*, 2014, **22**, 907–916.
48 S. Ravula, K. W. Wise, P. S. Shinde and J. E. Bara, Design and Performance of Di- and Tricationic Poly(ionic liquid) + Ionic Liquid Composite Membranes for CO_2 Separation, *Macromolecules*, 2023, **56**, 6126–6141.
49 T. Feng, B. Lin, S. Zhang, N. Yuan, F. Chu, M. A. Hickner, C. Wang, L. Zhu and J. Ding, Imidazolium-based organic–inorganic hybrid anion exchange membranes for fuel cell applications, *J. Membr. Sci.*, 2016, **508**, 7–14.
50 J. M. Lázaro Martínez, M. F. Leal Denis, V. Campo Dall'Orto and G. Y. Buldain, Synthesis, FTIR, solid-state NMR and SEM studies of novel polyampholytes or polyelectrolytes obtained from EGDE, MAA and imidazoles, *Eur. Polym. J.*, 2008, **44**, 392–407.
51 L. Burratti, M. Zannotti, V. Maranges, R. Giovannetti, L. Duranti, F. De Matteis, R. Francini and P. Prosposito, Poly(ethylene glycol) Diacrylate Hydrogel with Silver Nanoclusters for Water Pb(II) Ions Filtering, *Gels*, 2023, **9**, 133.
52 A. Tzereme, E. Christodoulou, G. Z. Kyzas, M. Kostoglou, D. N. Bikiaris and D. A. Lambropoulou, Chitosan Grafted Adsorbents for Diclofenac Pharmaceutical Compound Removal from Single-Component Aqueous Solutions and Mixtures, *Polymers*, 2019, **11**, 497.
53 V. S. Munagapati, V. Yarramuthi and D.-S. Kim, Methyl orange removal from aqueous solution using goethite, chitosan beads and goethite impregnated with chitosan beads, *J. Mol. Liq.*, 2017, **240**, 329–339.
54 R. Lafi, L. Abdellaoui, I. Montasser and A. Hafiane, Removal of methyl orange from aqueous solution onto modified extracted cellulose from *Stipa Tenacissima L*, *Int. J. Environ. Anal. Chem.*, 2022, **102**, 8124–8140.

55 M. S. Shamsudin, S. F. Azha, L. Sellaoui, M. Badawi, A. Bonilla-Petriciolet and S. Ismail, Performance and interactions of diclofenac adsorption using Alginate/Carbon-based Films: Experimental investigation and statistical physics modelling, *Chem. Eng. J.*, 2022, **428**, 131929.

56 L. A. Araujo, C. O. Bezerra, L. F. Cusioli, M. T. Rodríguez, R. G. Gomes and R. Bergamasco, Diclofenac adsorption using a low-cost adsorbent derived from Guazuma ulmifolia Lam. fruit via chemical and thermal treatment, *J. Environ. Chem. Eng.*, 2021, **9**, 106629.

57 K. Haitham, S. Razak and M. A. Nawi, Kinetics and isotherm studies of methyl orange adsorption by a highly recyclable immobilized polyaniline on a glass plate, *Arabian J. Chem.*, 2019, **12**, 1595–1606.

58 A. S. Poryvaev, K. P. Larionov, Y. N. Albrekht, A. A. Efremov, A. S. Kiryutin, K. A. Smirnova, V. Y. Evtushok and M. V. Fedin, UiO-66 framework with an encapsulated spin probe: synthesis and exceptional sensitivity to mechanical pressure, *Phys. Chem. Chem. Phys.*, 2023, **25**, 13846–13853.

59 Y. Lv, Z. Liang, Y. Li, Y. Chen, K. Liu, G. Yang, Y. Liu, C. Lin, X. Ye, Y. Shi and M. Liu, Efficient adsorption of diclofenac sodium in water by a novel functionalized cellulose aerogel, *Environ. Res.*, 2021, **194**, 110652.

60 F. G. L. M. Borsagli, V. S. T. Ciminelli, C. L. Ladeira, D. J. Haas, A. P. Lage and H. S. Mansur, Multi-functional eco-friendly 3D scaffolds based on N-acyl thiolated chitosan for potential adsorption of methyl orange and antibacterial activity against Pseudomonas aeruginosa, *J. Environ. Chem. Eng.*, 2019, **7**, 103286.

61 L. Tie, Y. Ke, Y. Gong, W. Zhang and Z. Deng, Nanocellulose fine-tuned poly(acrylic acid) hydrogel for enhanced diclofenac removal, *Int. J. Biol. Macromol.*, 2022, **213**, 1029–1036.

62 B. Satilmis and T. Uyar, Amine modified electrospun PIM-1 ultrafine fibers for an efficient removal of methyl orange from an aqueous system, *Appl. Surf. Sci.*, 2018, **453**, 220–229.

63 S. Zhuang, R. Cheng and J. Wang, Adsorption of diclofenac from aqueous solution using UiO-66-type metal-organic frameworks, *Chem. Eng. J.*, 2019, **359**, 354–362.

64 M. Hossein Beyki, M. Mohammadirad, F. Shemirani and A. A. Saboury, Magnetic cellulose ionomer/layered double hydroxide: An efficient anion exchange platform with enhanced diclofenac adsorption property, *Carbohydr. Polym.*, 2017, **157**, 438–446.

65 R. Huang, Q. Liu, J. Huo and B. Yang, Adsorption of methyl orange onto protonated cross-linked chitosan, *Arabian J. Chem.*, 2017, **10**, 24–32.

66 Y. Luo, X. Huang, S. Yao, L. Peng, F. Li and H. Song, Synthesis of a New Imidazole Amino Acid Ionic Liquid Polymer and Selective Adsorption Performance for Tea Polyphenols, *Polymers*, 2020, **12**, 2171.

67 J. Sun, Z. Jin, J. Wang, H. Wang, Q. Zhang, H. Gao, Z. Jin, J. Zhang and Z. Wang, Application of Ionic Liquid Crosslinked Hydrogel for Removing Heavy Metal Ions from Water: Different Concentration Ranges with Different Adsorption Mechanisms, *Polymers*, 2023, **15**, 2784.

68 U. Hwang, H. Moon, J. Park and H. W. Jung, Crosslinking and Swelling Properties of pH-Responsive Poly(Ethylene Glycol)/Poly(Acrylic Acid) Interpenetrating Polymer Network Hydrogels, *Polymers*, 2024, **16**, 2149.

69 J. Mercado-Montijo, D. M. Anstine, S. J. Rukmani, C. M. Colina and J. S. Andrew, PEGDA hydrogel structure from semi-dilute concentrations: insights from experiments and molecular simulations, *Soft Matter*, 2022, **18**, 3565–3574.

70 Z. Liu, R. Yu, S. Zeb, Q. Tao, H. Li, J. Wang, L. Xiang, S. Ya, J. Li and Y. Liu, Preparation and Adsorption Properties of a Three-Dimensional Superhydrophilic Mercury-Ion-Imprinted Polymer with Dual Recognition Site Based on MoS_2 /SBA-15, *Inorg. Chem.*, 2024, **63**, 23705–23724.

71 X. Zhang, T. Wu, Y. Zhang, D. H. L. Ng, H. Zhao and G. Wang, Adsorption of Hg^{2+} by thiol functionalized hollow mesoporous silica microspheres with magnetic cores, *RSC Adv.*, 2015, **5**, 51446–51453.